

Strong spin-lattice coupling and high-temperature magnetic ordering in monolayer chromium dichalcogenides

A. González-García ^{1,2} C. Bacaksiz ^{2,3,4} T. Frauenheim,^{4,5,6} and M. V. Milošević^{2,7,*}

¹*Grupo de Investigación en Física Aplicada, Departamento de Física, Universidad del Norte, Barranquilla 081007, Colombia*

²*Department of Physics & NANOLab Center of Excellence, University of Antwerp, Groenenborgerlaan 171, 2020 Antwerp, Belgium*

³*Computational Biotechnology, RWTH Aachen University, Worringerweg 3, 52074 Aachen, Germany*

⁴*Bremen Center for Computational Material Science (BCCMS), D-28359 Bremen, Germany*

⁵*Shenzhen JL Computational Science and Applied Research Institute, Shenzhen 518131, China*

⁶*Beijing Computational Science Research Center, Beijing 100193, China*

⁷*Instituto de Física, Universidade Federal de Mato Grosso, Cuiabá, Mato Grosso 78060-900, Brazil*



(Received 17 October 2023; accepted 25 April 2024; published 13 June 2024)

We detail the magnetic properties of monolayer CrX_2 and its Janus counterparts CrXY ($X, Y = \text{S, Se, Te}$, with $X \neq Y$) using *ab initio* methods and Landau-Lifshitz-Gilbert magnetization dynamics, and uncover the pronouncedly strong interplay between their structure symmetry and the magnetic order. The relaxation of non-magnetic chalcogen atoms, that carry large spin-orbit coupling, changes the energetically preferential magnetic order between in-plane antiferromagnetic and tilted ferromagnetic one. The considered Janus monolayers exhibit sizable Dzyaloshinskii-Moriya interaction, in some cases above 20% of the isotropic exchange, and critical temperature of the long-range magnetic order in the vicinity or even significantly above the room temperature.

DOI: [10.1103/PhysRevMaterials.8.064001](https://doi.org/10.1103/PhysRevMaterials.8.064001)

I. INTRODUCTION

Most two-dimensional (2D) materials are not magnetic in their pristine form. Thermal fluctuations suppress long-range magnetic order in monolayers at any nonzero temperature [1,2], unless that detrimental effect of fluctuations is neutralized by the presence of magnetic anisotropy, which can be induced in a 2D crystal by, e.g., doping with transition metals [3–6]. The microscopic source of magnetic anisotropy is the spin-orbit coupling (SOC), which is sizable in all the magnetic 2D materials realized to date, starting from the pioneering discoveries of long-range magnetism in monolayer CrI_3 [7] and CrGeTe_3 [8] (for a recent review, see [9]). When the spin-orbit coupling is combined with a broken spatial inversion symmetry, the Dzyaloshinskii-Moriya interaction (DMI) arises within the magnetic material [10,11]. DMI is an antisymmetric magnetic exchange interaction that orients the neighboring spins orthogonally to each other, with a unique sense of rotation, instead of the (anti)parallel spin alignments stemming from the usual Heisenberg exchange interaction [12].

In parallel with the rise of 2D magnetic materials, recent years have witnessed the advent of Janus monolayers. Named after a two-faced god from Roman mythology, Janus 2D materials have different top and bottom surfaces, which breaks the mirror symmetry and instigates their unique physical, chemical, and quantum properties, promising for many potential applications [13–16]. Janus transition-metal dichalcogenide (JTMDC) monolayers (MXY , where $M = \text{Mo, W}$ and $X, Y = \text{S, Se, Te}$, with $X \neq Y$), have been theoretically found to be dynamically stable [15,17] and were experimentally synthesized [18,19]. Despite the strong Rashba SOC in these

materials, long-range magnetism was not observed. Magnetic Janus 2D materials are expected to host strong intrinsic polarization and piezoelectric response, coupled to pronounced Dzyaloshinskii-Moriya interaction (DMI), which would recommend them for diverse multifunctional applications in spintronics, memory, logic, and magnetoelectric devices. To date, 2D Janus $\text{Cr}_2\text{Cl}_3\text{I}_3$ has been reported to be a ferromagnetic (FM) semiconductor material with a direct band gap [20], and strong emergent DMI has been predicted in 2D Janus manganese dichalcogenides MnXY ($X, Y = \text{S, Se, Te}$, with $X \neq Y$) [21,22], VSeTe [22], and $\text{Cr}(\text{I}, X)_3$ ($X = \text{Br, Cl}$) [23] by first-principles calculations [21]. Recently, two-dimensional Cr-based dichalcogenide halides CrYX (where $Y = \text{S, Se, Te}$ and $X = \text{Cl, Br, I}$) have demonstrated appealing multifunctional capabilities in the domain of topological electronic and valleytronic device applications [24].

Since monolayer 1T-CrS_2 [25,26], CrSe_2 [26–28], and CrTe_2 [26,29–31] crystals have been successfully synthesized, and recently a room-temperature ferromagnetism has been found in 2D CrTe_2 films [31], the prospects of experimental realization of the magnetic Janus CrXY ($X, Y = \text{S, Se, Te}$, with $X \neq Y$) are growing by the day. He *et al.* have theoretically investigated the physical properties of such chromium Janus dichalcogenides using first-principle methods [32]. However, the structural changes and the corresponding variety of the emergent magnetic interactions and possible noncollinear orderings were not considered, which calls for a more rigorous study. Therefore, motivated by above-mentioned developments and prospects, we here detail the structural, electronic, and magnetic properties of 2D CrX_2 and their Janus counterpart CrXY monolayers ($X, Y = \text{S, Se, Te}$, with $X \neq Y$) using relativistic density-functional calculations. In doing so, we reveal the particularly strong spin-lattice coupling, high-temperature long-range magnetic order, and

*milorad.milosevic@uantwerpen.be

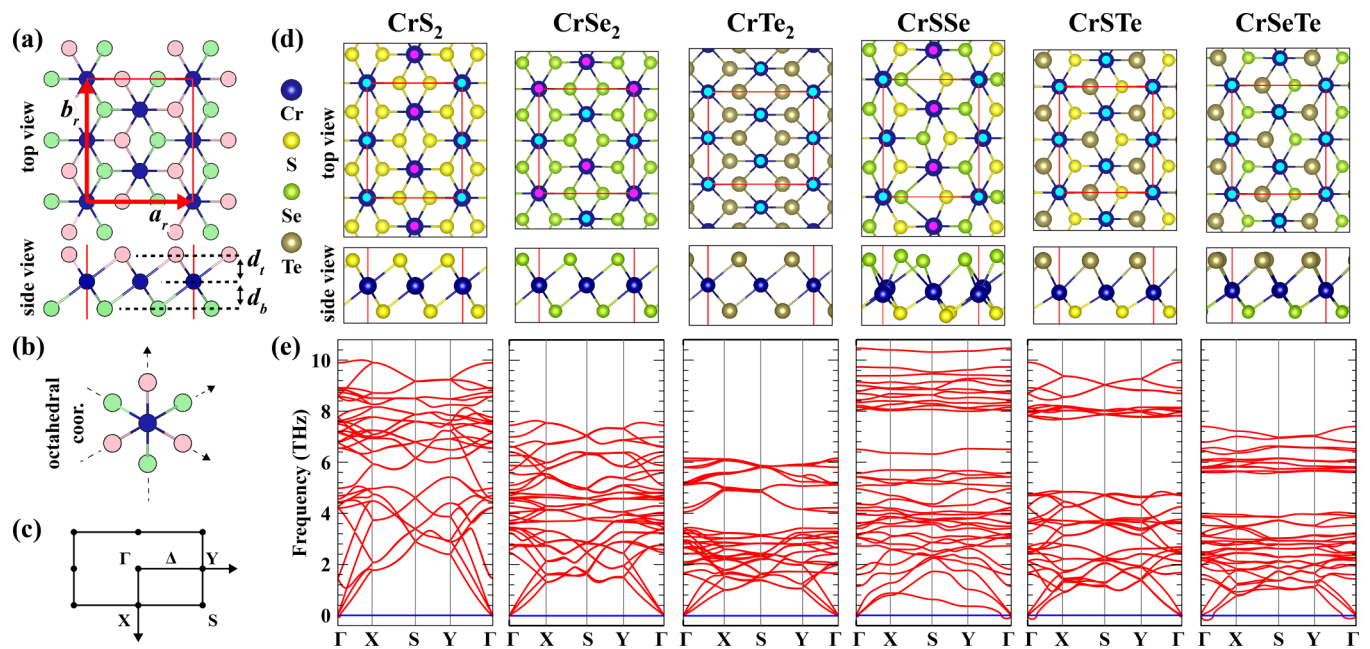


FIG. 1. Schematic representation for (a) top view of the rectangular unit cell for CrX_2 ($X = \text{S}, \text{Se}, \text{Te}$); blue atoms denote Cr, and green (pink) ones show the chalcogen atoms (S, Se, Te) of the bottom (top) surface. $a_r(x)$ and $b_r(y)$ are the lattice vectors; d_t (d_b) denotes the distance between the Cr layer and top (bottom) chalcogen layer. (b) Octahedral coordination of each Cr atom, and (c) top view of the high symmetry points in the Brillouin zone for the rectangular unit cell of (J)TMDCs. (d) Top and side views of the considered TMDC and JTMDC systems, with atoms denoted by color as shown on the left. The individual magnetic moments of the ground-state magnetic order are shown on Cr atoms as purple (spin down) and cyan dots (spin up). (e) Phonon band structures of the monolayers shown in (d).

sizable DMI, which in combination with polarization due to symmetry breaking makes these materials a uniquely versatile magnetoelectronic playground worthy of further experimental effort. Our research also uncovers various types of unique 2D magnetic ground states in chromium-based Janus materials, such as the ferromagnetic (antiferromagnetic) semiconductor CrSSe and the ferromagnetic metals CrSTe and CrSeTe, that may assist further advances of magnetic memory technology and spintronics applications of 2D materials and their heterostructures [33,34].

II. COMPUTATIONAL DETAILS

The analysis of structural, phonon, electronic, and magnetic properties of Cr-based TMDCs and JTMDCs was carried out using relativistic density-functional theory calculations [35,36]. The Perdew-Burke-Ernzerhof functional [37] was used to treat the electron exchange-correlation interactions. The ion-electron interactions were described by the projector augmented wave (PAW) method [38,39], implemented in the Vienna *ab initio* simulation package (VASP) [40,41]. For optimization of the lattice parameters, the electron wave function was expanded in plane waves up to a cutoff energy of 700 eV, and a Γ -centered grid of $6 \times 6 \times 1$ k points was used to sample the irreducible Brillouin zone. The geometric convergence criterion for energy was set at 10^{-7} eV. Furthermore, the Grimme's method (DFT-D2) was used to treat long-range electronic correlations [42]. Due to the possible existence of the polarization dipole in Janus CrXY monolayers, the dipole correction is taken into account. To avoid the periodic interactions, a 20 Å vacuum was kept as vertical spacing between

the adjacent layers. The spin-orbit interaction (SOC) is fully considered. On-site Coulomb interactions of $3d$ -Cr orbitals were taken into account using the DFT + U [43] approach. U parameters of each considered monolayer were obtained separately using a linear response method [44], as 3.72, 3.90, 3.79, 3.81, 3.75, and 3.84 eV for CrS₂, CrSe₂, CrTe₂, CrSSe, CrSTe, and CrSeTe, respectively. In order to examine the dynamical stability of our systems, we calculated the phonon dispersion using PHONOPY [45], based on the finite-displacement method (FDM) [46,47]. First-principles phonon calculations were performed by taking into account the interactions in $3 \times 3 \times 1$ supercells consisting of 36 Cr atoms and 72 chalcogen atoms. To obtain magnetic exchange interactions between Cr atoms and the single-ion anisotropy, we employed the four-state energy mapping (4SM) methodology [48,49]. The magnetic ground state and the temperature-dependent magnetization were then calculated using the atomistic spin simulation code SPIRIT, based on the Landau-Lifshitz-Gilbert (LLG) formalism [50].

III. RESULTS AND DISCUSSION

A. Structural and electronic properties

Pristine TMDC monolayers 1T- CrX_2 ($X = \text{S}, \text{Se}, \text{Te}$) have the triangular lattice layer of Cr atoms sandwiched between the two triangular lattices of the chalcogen atoms in A-B-C stacking, as shown in Fig. 1(a). Cr atom exhibits octahedral coordination [O_h], shown in Fig. 1(b)]. As three different chalcogen atoms are considered in our study, the three different Janus CrXY monolayers were examined: CrSSe, CrSTe, and CrSeTe. In order to depict possible distortions

TABLE I. Calculated structural parameters of pristine and Janus Cr-dichalcogenide monolayers. $a_r(x)$ and $b_r(y)$ are the lattice vectors of the rectangular unit cell. $n = \frac{a_r}{b_r} / \frac{\sqrt{3}}{2}$ illustrates the deviation of the lattice structure from the ideal triangular lattice. d_t and d_b are the respective distances of the Cr layer from the top and bottom chalcogen layers. Ratio d_t/d_b then reflects the vertical symmetry breaking in the structure. ρ_t and ρ_b are the charge transfers between the Cr and top and bottom chalcogen atoms respectively. m , in units of Bohr magneton μ_B , is the on-site magnetic moment. MS is the lowest-energy magnetic configuration among the considered magnetic orders in the DFT scheme: s-, z-, out-, and in- stand for stripy, zig-zag, out-of-plane, and in-plane, respectively. ES gives the electronic state, i.e., metallic (m) or semiconductor (s).

	a_r (Å)	b_r (Å)	n	d_t (Å)	d_b (Å)	d_t/d_b	ρ_t (e)	ρ_b (e)	m (μ_B)	MS	ES
CrS ₂	5.51	6.67	0.95	1.49 (S)	1.49 (S)	1.00	0.59 (S)	0.59 (S)	2.5	s-AFM	m
CrSe ₂	6.01	6.61	1.05	1.63 (Se)	1.63 (Se)	1.00	0.51 (Se)	0.51 (Se)	2.7	z-AFM	m
CrTe ₂	7.32	6.42	1.32	1.78 (Te)	1.78 (Te)	1.00	0.42 (Te)	0.42 (Te)	3.2	out-FM	m
CrSSe	5.66	6.94	0.94	1.91 (Se)	1.32 (S)	1.45	0.43 (Se)	0.71 (S)	3.0	s-AFM	s
CrSTe	6.07	6.87	1.02	2.06 (Te)	1.24 (S)	1.66	0.36 (Te)	0.71 (S)	2.9	out-FM	m
CrSeTe	6.17	7.14	1.00	1.98 (Te)	1.42 (Se)	1.39	0.37 (Te)	0.59 (Se)	3.0	in-FM	m

and/or reconstructions, we considered a rectangular unit cell with four Cr and eight chalcogen atoms. The structural analyses of those six monolayer materials were done by including spin-orbit coupling and considering the ferromagnetic (FM), zig-zag antiferromagnetic (z-AFM), and stripy antiferromagnetic (s-AFM) states. While keeping the considered magnetic order fixed, the atomic positions as well as the lattice vectors of the structure were optimized, and the energies of all the possible magnetic states (with converged structure) were compared. In Table I, we list the so-obtained structural parameters and the corresponding lowest-energy magnetic states for each of the systems. Note that the shown and listed magnetic states are the lowest energy ones among the three considered magnetic orders. The structure with the lowest energy is used for magnetic exchange interaction calculations. The obtained magnetic exchange parameters are used in LLG spin simulations to determine the magnetic ground states, which are compared with the states listed in Table I. It is worth mentioning that, among the six materials studied here, Janus CrSSe stands out due to several distinctive characteristics. First, it exhibits notable changes in the structure depending on the magnetic order. Second, it is the only material exhibiting a semiconducting nature. Lastly, in contrast to initial DFT analysis, it exhibits a FM magnetic ground state achievable through the LLG scheme further in the investigation. Each of these aspects is discussed in detail in its respective section.

As shown in Fig. 1, each material maintains triangular lattice and octahedral coordination of the Cr atoms. However, the in-plane symmetry is broken in each structure. In addition, the out-of-plane symmetry is broken for the Janus structures. In order to quantify in-plane asymmetry, we define a parameter $n = \frac{a_r}{b_r} / \frac{\sqrt{3}}{2}$ [the normalized ratio between lattice vectors, a_r/b_r , with respect to that of the perfect triangular lattice ($\sqrt{3}/2$)], and listed its values for the ground states of different materials in Table I. The lattice sizes increase with the size of the chalcogen atoms, as expected. The in-plane asymmetry parameter, n , on the other hand, also increases for the pristine structures. However, for the Janus ones, it changes slightly and remains close to 1, which is the value of the perfect triangular lattice. To reveal the interplay between the structure symmetry and the magnetic order even more clearly, in Table II we list the values of the in-plane asymmetry parameter of the pristine

and Janus structures for different considered magnetic orders. All structures except CrTe₂ exhibit significant variation in parameter n with magnetic order, which demonstrates the *strong spin-lattice coupling in these compounds*. We will return to this important point again in the discussion further down the article.

Another parameter that shows the structural changes is the out-of-plane asymmetry. In Table I, the distances between the Cr layer and the top or bottom chalcogen layer (d_t or d_b , respectively) and their ratios (d_t/d_b) are given. The pristine monolayers are symmetric in the out-of-plane direction. Those distances increase with increasing size of the involved chalcogen. Specifically, the distances between the layers of Cr and S atoms and Cr and Se atoms in CrS₂ and CrSe₂ are 1.49 and 1.63 Å, respectively. However, in the Janus CrSSe, the corresponding distances are 1.32 and 1.91 Å, respectively. Such a trend also exists in other layers and their Janus counterparts. In short, in Janus monolayers the Cr-chalcogen distance decreases (increases) compared to the pristine monolayer case when the chalcogen atom at the opposite side is larger (smaller). The most asymmetric case is CrSTe with $d_t/d_b = 1.66$. Our Bader charge analyses align with the behavior of the atomic layer distances (d_t and d_b). S, Se, and Te atoms accept $0.59e$, $0.51e$, and $0.42e$ from the Cr atom in pristine monolayer cases, respectively. In general, the shorter bond length indicates the larger charge transfer. In the Janus cases, the charge transfer decreases (increases) when

TABLE II. The in-plane asymmetry parameter, n , of the pristine and Janus structures of Cr-dichalcogenide monolayers with different magnetic orders. $n = \frac{a_r}{b_r} / \frac{\sqrt{3}}{2}$ [the normalized ratio between lattice vectors, a_r/b_r , with respect to that of the perfect triangular lattice ($\sqrt{3}/2$)].

	FM	z-AFM	s-AFM
CrS ₂	1.00	1.02	0.95
CrSe ₂	0.98	1.05	0.92
CrTe ₂	1.32	1.29	1.30
CrSSe	0.99	1.05	0.94
CrSTe	1.02	0.94	0.92
CrSeTe	1.00	0.93	0.92

the chalcogen atom on the opposite side is larger (smaller). Similar trends for the lattice constant and the bond length were reported in earlier studies of 2D Janus monolayer structures [21,51]. As mentioned above, the Janus CrSSe particularly differs from the others due to the significantly distorted octahedral coordination of the Cr atoms alongside the buckled form of the Cr layer, as seen in Fig. 1(d). In the unit cell of CrSSe, two out of the four Cr atoms exhibit a more pronounced change in their octahedral coordination. Despite these structural modifications, each Cr atom maintains the same magnetic moment, indicative of identical orbital occupancy. Remarkably, the magnetic moment is found to be $3\mu_B$, which deviates from the expected values since the pristine Cr-dichalcogenide counterparts exhibit $2.5\mu_B$ and $2.7\mu_B$ for CrS₂ and CrSe₂, respectively. In addition, the electronic character of CrSSe is semiconducting, thus different from the metallic state observed in both base pristine materials. This behavior also contrasts with that obtained in other pristine and Janus Cr-dichalcogenide materials. The reconstruction or distortion, accompanied by the electronic transition, suggests that a Jahn-Teller type mechanism occurs in CrSSe. Such reconstructions typically lead to a more disordered structure and a reduction in the total energy of the system. Regarding the possible question of why CrSSe exhibits such a reconstruction while other Janus CrXY monolayers do not, we attribute this physical feature to the difference of electronegativity between S, Se, and Te. Structural distortions in materials can arise due to various factors, such as chemical bonding preferences due to difference of electronegativity. In the case of Janus CrXY materials, and based on the difference of electronegativity values of Cr (1.6), S (2.5), Se (2.4) and Te (2.1), and the fact that S has higher electronegativity compared to Se and Te, and the lower electronegativity of Te relative to S or Se, one would expect a higher degree of polarity in Cr-SSe bonds relative to Cr-STe and Cr-SeTe bonds. This higher polarity may induce stronger local distortions in the CrSSe structure, as the chromium atom strives to maintain equilibrium between its interactions with the more electronegative sulfur and the less electronegative selenium. Conversely, the structural distortions in CrSTe and CrSeTe would be less pronounced due to a more balanced distribution of electron density between the chromium and chalcogen atoms.

To validate the stability of the obtained structures, vibrational (phonon) calculations were performed, with results shown in Fig. 1(e). In general, there are no imaginary frequencies in the phonon dispersion, except for weak deviations at around the Γ point in some cases that are likely due to insufficiently large supercell (limited by the computational load). This feature has been found in other 2D Janus systems [17,52], is usually discarded as a technicality, and highlights the flexural acoustic mode of these materials. Moreover, since the 2D JTMDs are synthesized on the substrate [17,18,52], any bending instability would be voided in reality. We thus conclude that the presented phonon dispersions validate the stability of each considered structure. The reduction of the frequency levels of the phonon bands as the size of the chalcogen atoms increases indicates that the bonds are also softening with the size of the atoms involved.

As mentioned above, our structural analysis shows that structural properties of the considered Cr-dichalcogenides

strongly depend on the established magnetic order (be it FM, z-AFM, or s-AFM) and vice versa. Considering the magnetic state shown in Fig. 1(d), the lattice tends to expand in the direction of ferromagnetically aligned chains while it is compressed in the direction of the antiferromagnetic chains. Such behavior is evident in all the AFM systems.

With regard to the reported electronic properties of the 1T-CrX₂ in the literature, all of them are observed to be metallic [27,31,53–57]. Indeed, in all our CrX₂ structures, a metallic character is found, as shown in Fig. 2. On the other hand, we found that 2D Janus CrSSe is a Y- Δ indirect semiconductor [see Figs. 2 and 1(c)], with a band gap in the infrared electromagnetic spectrum (0.80 eV) and a direct (Y-Y) optical transition at 0.82 eV. This intrinsic ferromagnetic yet semiconducting nature of CrSSe, which is scarce in the literature, is interesting for potential applications in optospintronic nanodevices [58,59]. Conversely, our results show that both CrSTe and CrSeTe are also ferromagnetic but metallic in nature. This prediction of various 2D magnetic Janus systems, ranging from ferromagnetic semiconductor to ferromagnetic metals, which are likely highly responsive to external stimuli, suggests their prospective applications in multifunctional magnetic nanodevices, including magnetic memory-based devices [33,34,60] and sensors. [61] Furthermore, the semiconducting ferromagnetic Janus monolayer, with its intrinsic dipole moment, holds great potential for inducing intriguing spin states in graphene through proximity effects. Furthermore, the predicted semiconducting ferromagnetic Janus monolayer, with its intrinsic dipole moment, holds great potential for inducing intriguing spin states in graphene through the proximity effect, useful for realizing spin-current generation for prospective 2D logic applications [62,63].

B. Magnetic properties

Next we discuss the magnetic properties of the considered monolayers in greater detail. Since the considered 2D materials exhibit distorted structures, even the pristine dichalcogenide ones, the magnetic interactions are expected to vary depending on the chosen pair of Cr atoms. Therefore, every unique pair is determined based on the interatomic distance (down to 10^{-3} Å precision). Then the corresponding magnetic exchange interaction matrix is calculated, using the four-state methodology. In Table III we list the obtained exchange parameters for all the calculated Cr pairs (i, j), labeled according to Fig. 3. In order to isolate the considered pair from its repeating image in the periodic system, we used the supercell approach (each Cr pair was calculated using a 2×2 supercell). The interaction matrices of the unlisted pairs were determined by rotation operation on that of obtained pairs with the same distance.

In monolayer CrS₂, the magnetic interaction matrices of two distinct pairs of Cr atoms (cf. Table III and Fig. 3) are sufficient to define the magnetic interaction throughout the material. We found that the diagonal elements of the interaction matrices, which correspond to symmetric-isotropic interaction, for both Cr pairs have antiferromagnetic (AFM) nature, where in-plane components are slightly larger than the out-of-plane ones. That feature is visualized in the temperature-dependent coordinate-decomposed magneti-

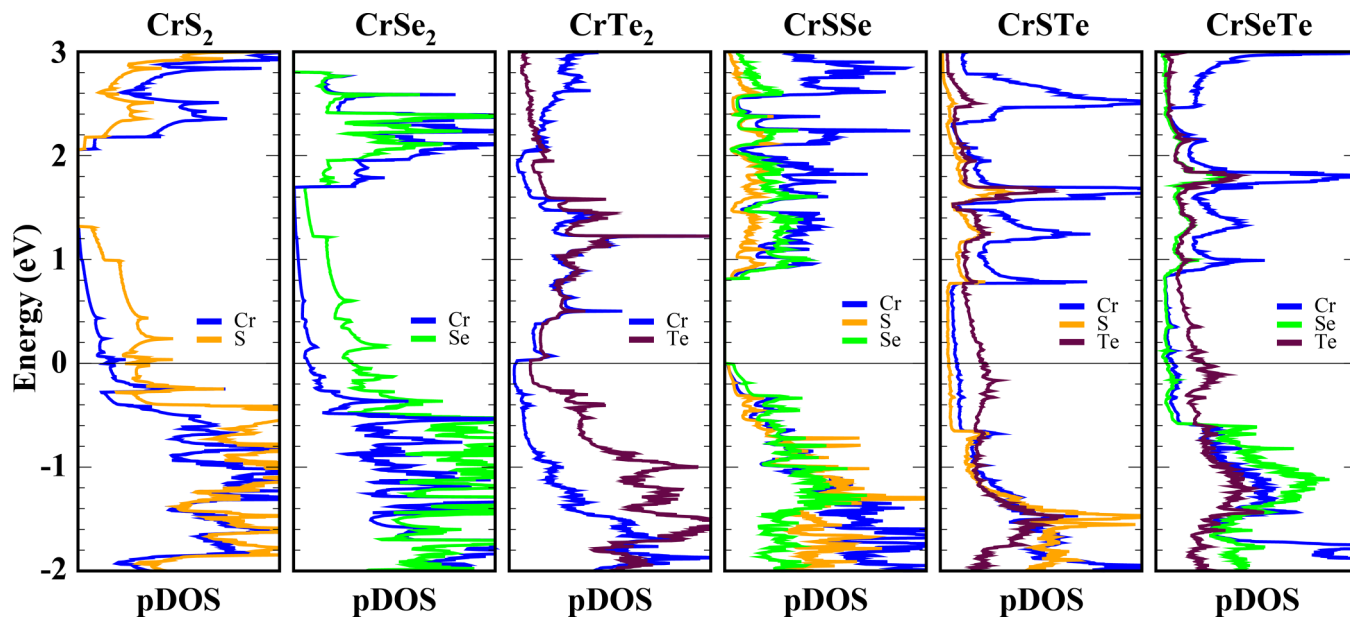


FIG. 2. Projected density of states (pDOS) of the Cr (blue), S (orange), Se (green), and Te (brown) atoms for the considered CrXY ($X, Y = S, Se, Te$) magnetic systems, calculated with SOC included. Fermi energy is set to 0 eV.

zation in Fig. 4. Cr-1 and Cr-2 exhibit parallel magnetic moments, and they are anti-parallel to the aligned magnetic moments of Cr-3 and Cr-4. The phase transition from paramagnetic to antiferromagnetic order occurs at $T_c = 222$ K and the system ends up with in-plane stripy AFM (*s*-AFM) configuration at $T = 0$ K, as shown in Fig. 4. This is consistent with the previous reports based on DFT analysis [53]. Monolayer CrSe₂ has three uniquely different pairs, where one exhibits strong FM interaction along a zig-zag chain of Cr, while the other two pairs have weak AFM interaction. Together, such interactions foster a zig-zag AFM (*z*-AFM) configuration below the (rather low) T_c of 52 K. At $T = 0$, the magnetic moments are slightly tilted in the *x* and *y* directions. In the last considered pristine dichalcogenide, CrTe₂, two unique pairs

are found to be sufficient to describe magnetic interactions; while both show FM interaction, one is stronger than the other, the FM long-range order is established below $T_c = 186$ K, and the system exhibits a tilted (*t*-*xyz*, thus tilted in all directions) FM configuration at $T = 0$ K. In preceding work, Lv *et al.* found FM and AFM orderings in CrTe₂ and CrSe₂ monolayers respectively, based on a first-principles study. They also reported that magnetic properties can be tuned by strain, i.e., strain induces a switch from FM (AFM) to AFM (FM) state in a CrTe₂ (CrSe₂) monolayer [56]. Furthermore, Xiuxian *et al.* reported a FM ground state for a CrTe₂ monolayer [57]. Monolayer CrTe₂ was recently experimentally grown on bilayer graphene by molecular beam epitaxy (MBE) and was reported to be FM with a T_c of ~ 200 K [31]. Our results show agreement with these studies. Conversely, Xian *et al.* observed a stable AFM order [30] in a CrTe₂ monolayer grown on a SiC supported bilayer graphene. These discrepancies between experimental results regarding the magnetic ground state of CrTe₂ could be attributed to different interfacial strain and/or substrate temperature.

Regarding the magnetic properties of the Janus layers, we commence with CrSSe. As mentioned in the structural analysis, CrSSe is visually the most intrinsically deformed monolayer among the considered ones. As a consequence, seven unique Cr-pairs need to be considered to properly describe magnetic interactions throughout the monolayer. All those pairs were found to exhibit FM interaction, varying from very weak (~ -0.25 meV) to very strong (~ -15 meV). This set of exchange interactions results in T_c of 268 K of the FM state, as shown in Fig. 4. FM interaction at all pairs and the resultant FM magnetic state at $T = 0$ K from the LLG simulations were not expected, since we found the *s*-AFM state as the lowest-energy configuration in the DFT scheme. In order to test this peculiar result, we returned to the DFT routine and considered FM configuration on the structure obtained for *s*-AFM order, which indeed delivered lower energy

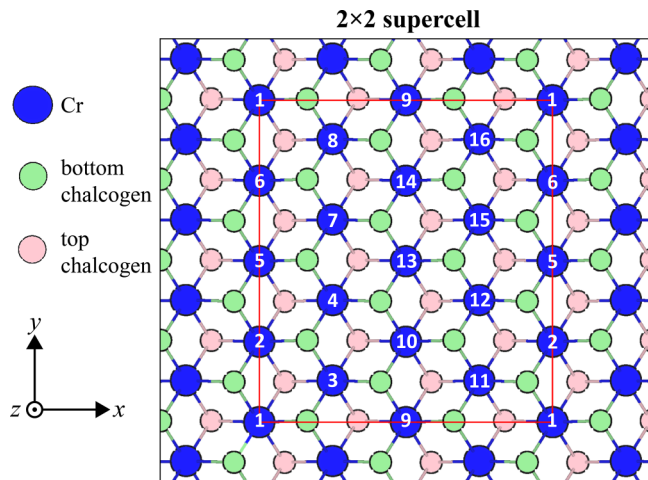


FIG. 3. Schematic depiction of the considered supercell in the magnetic exchange interactions calculations, with indices of the atoms shown. 2×2 supercell is used to calculate the exchange interaction of each Cr pair.

TABLE III. Pair (i, j) stands for the unique pair of i th and j th atoms. $d(i, j)$ is the atomic distance between the (i, j) pair. The calculated magnetic exchange interaction parameters are as follows: the isotropic exchange (the diagonal elements of the interaction matrix), J_{ij}^x, J_{ij}^y and J_{ij}^z ; the DMI vector components $D_{ij}^x, D_{ij}^y, D_{ij}^z$, and modulus $|D|$; the ratio between the DMI and the average isotropic interaction $|D|/\langle J_{ij} \rangle$; the magnetic moment m of Cr, in units of Bohr magneton μ_B ; A_i^z , the zz element of the single-ion anisotropy matrix for the i th Cr atom, ranging from Cr₁ to Cr₄ as the repeating Cr sites in the supercell consideration; a positive (negative) value indicates a preference for in-plane (out-of-plane) orientation, respectively; the critical temperature T_c ; and the magnetic ground state (MGS) at $T = 0$. s- and z- indicate stripy and zig-zag, respectively; in- and t- indicate in-plane and tilted, respectively, referring to the axes x, y , and z for the components of the magnetization at $T = 0$ K. xy denotes that the magnetization exhibits components only on the x and y directions, while xyz indicates that the magnetization exhibits components in all three coordinate directions. Nomenclature of the pairs (i, j) is shown in Fig. 3.

	Pair (i, j)	$d(i, j)$ (Å)	J_{ij}^x (meV)	J_{ij}^y (meV)	J_{ij}^z (meV)	D_{ij}^x (meV)	D_{ij}^y (meV)	D_{ij}^z (meV)	$ D $ (meV)	$ D /\langle J_{ij} \rangle$	Site (i)	A_i^z (meV)	m (μ_B)	T_c (K)	MGS ($T = 0$ K)
CrS ₂	(1,2)	3.333	-3.47	-3.47	-3.30	0	0	0	0	0	(1)	-0.12	2.5	222	s-AFM (x)
	(1,3)	3.220	8.38	8.37	8.31	0	0	0	0	0	(2)	-0.12			
											(3)	-0.12			
CrSe ₂	(1,2)	3.303	5.85	5.75	6.39	0	0	0	0	0	(1)	0.30	2.7	52	z-AFM (z)
	(1,3)	3.457	-2.36	-2.30	-2.07	0	0	0	0	0	(2)	0.29			
	(2,3)	3.400	-0.92	-0.89	-0.58	0	0	0	0	0	(3)	0.31			
											(4)	0.30			
CrTe ₂	(1,2)	3.213	-1.32	-1.89	-1.27	0	0	0	0	0	(1)	0.22	3.2	186	FM (t-xyz)
	(1,3)	3.999	-6.79	-6.24	-7.05	0	0	0	0	0	(2)	0.22			
											(3)	0.23			
CrSSe	(1,2)	3.398	-9.92	-9.93	-9.92	-0.29	-0.11	-0.10	0.33	0.03	(1)	0.02	3.0	268	FM (t-xyz)
	(1,3)	3.264	-12.55	-12.56	-12.52	-0.11	0.11	0.28	0.32	0.03	(2)	-0.01			
	(2,3)	3.457	-0.25	-0.24	-0.24	0.06	0.08	0.13	0.16	0.67	(3)	-0.02			
	(3,4)	3.499	-15.63	-15.71	-15.70	0.06	0.00	0.23	0.24	0.02	(4)	-0.02			
	(3,9)	3.186	-9.53	-9.351	-9.50	0.16	0.10	0.05	0.20	0.02					
	(3,10)	3.460	-6.83	-6.86	-6.84	0.07	0.12	0.04	0.14	0.02					
	(4,7)	3.484	-8.82	-8.87	-8.81	-0.16	-0.01	-0.04	0.17	0.02					
CrSTe	(1,2)	3.435	-10.22	-10.56	-10.33	-0.46	0.01	0.31	0.55	0.05	(1)	-0.20	2.9	319	FM (in-xy)
	(1,3)	3.488	-11.50	-11.50	-11.56	-0.35	0.51	-0.25	0.67	0.06	(2)	-0.43			
											(3)	-0.18			
											(4)	-0.20			
CrSeTe	(1,2)	3.537	-9.26	-9.55	-9.35	-1.18	-0.24	0.39	1.27	0.13	(1)	0.23	3.0	268	FM (y)
	(1,3)	3.552	-13.22	-13.30	-13.28	-0.22	0.94	0.83	1.27	0.10	(2)	0.15			
	(1,8)	3.534	-9.53	-9.61	-9.13	0.82	1.02	0.44	1.38	0.15	(3)	0.16			
	(1,16)	3.526	-11.67	-11.71	-11.40	0.59	-0.85	-0.71	1.25	0.11	(4)	0.27			
	(2,3)	3.590	-5.86	-5.97	-5.69	0.46	0.95	-0.41	1.13	0.19					
	(2,4)	3.576	-6.20	-6.12	-6.07	-0.53	0.83	0.39	1.06	0.17					
	(2,5)	3.508	-8.70	-9.07	-8.61	-1.10	0.24	-0.33	1.17	0.13					
	(3,4)	3.624	-9.24	-9.52	-9.31	-1.10	0.24	-0.39	1.19	0.13					
	(3,9)	3.504	-6.24	-6.17	-6.09	0.52	0.83	-0.83	1.28	0.21					
	(3,10)	3.604	-5.86	-5.96	-5.69	-0.46	0.95	0.41	1.13	0.19					
(4,7)	3.621	-8.59	-8.92	-8.53	-1.01	-0.35	-0.31	1.11	0.13						
(4,10)	3.610	-13.20	-13.28	-13.22	0.26	0.94	-0.83	1.28	0.10						

than what we had previously, and also lower energy than the FM state with nearly perfect 1T structure (which was found to be unstable). Figure 5 shows the three lowest-energy states, for three different magnetic orders, and three different degrees of deformation, once again demonstrating a strong interplay between magnetic order and the structural symmetry in this material.

The other two monolayers we studied, CrSTe and CrSeTe, exhibit FM order with T_c of 319 and 268 K, respectively. Our findings for CrSTe and CrSeTe are consistent with those reported by Cui *et al.* [64]. The magnetic configuration of CrSTe at $T = 0$ K for both layers, as obtained in LLG simulations, is FM, as was also found in the DFT scheme, yet it is in-plane. Considering that the energy difference between in-plane and

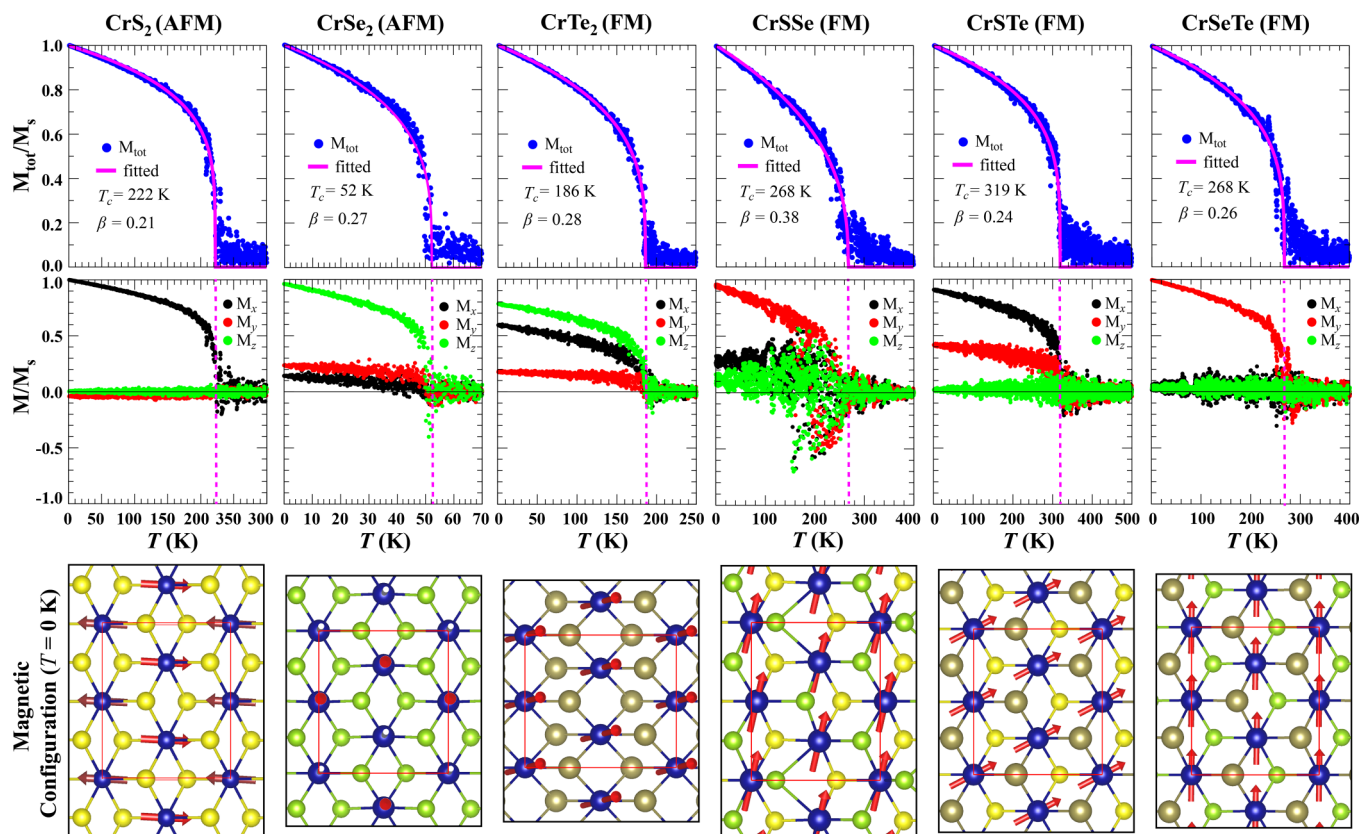


FIG. 4. Temperature-dependent normalized magnetization obtained via LLG simulation, based on the magnetic interaction parameters given in Table III, for the ground-state magnetic order shown in the bottom-most panel. In the case of a FM ground state, the upper and lower top panels show the total and the coordinate-decomposed magnetization, respectively. In the case of an AFM order, in those panels the magnetization of one of the FM subconfigurations is plotted, since the total magnetization is zero.

out-of-plane FM configurations in the DFT scheme is only ~ 0.25 meV/f.u., such deviation is plausible. On the other hand, CrSeTe exhibits a magnetic moment which is in-plane pointing y direction as it is obtained in the DFT analysis.

Further regarding the Janus monolayers, a strong DMI is expected to arise since the inversion symmetry that Cr pairs see is broken between the top and bottom chalcogens, and also due to the distortion of the octahedral coordination. Our calculated values of DMI magnitude $|D|$ and its ratio to the average isotropic exchange, $|D|/\langle J_{ij} \rangle$, of the given Cr pair (i, j) are listed in Table III. The Janus CrSSe, which is the

most intrinsically distorted among the studied monolayers, exhibits weak $|D|$, on average ≈ 0.22 meV. This is just 2.5% of the average isotropic exchange interaction of $-$ meV. For instance, $9.08|D|/\langle J_{ij} \rangle$ is found to be 67% for the (2,3) pair of CrSSe. However, $\langle J_{ij} \rangle$ is also weak for that pair, therefore there is no significance of that large ratio in the magnetic properties. The Janus CrSTe monolayer exhibits stronger average $|D|$ of 0.61 meV as compared to CrSSe, but the $\langle J_{ij} \rangle$ is also stronger, resulting in still small $|D|/\langle J_{ij} \rangle$ ratio of about 6% in average. The strongest DMI is found in Janus CrSeTe monolayer, having amplitude of 1.21 meV on average, which corresponds to 15% of -8.98 meV of the average isotropic exchange. This large ratio stands out when compared to those of the Cr(I, Br)_3 (27%) and Cr(I, Cl)_3 (29.40%) Janus monolayers [23], since the corresponding exchange interactions are relatively small in those materials, and suggests formation of noncollinear spin textures in the ground state. Our results for CrSTe and CrSeTe agree with those of a recent theoretical study of 2D Janus chromium dichalcogenides under strain [64]. The latter study showed that the CrSTe monolayer has high T_c of 295 K and an out-of-plane magnetic anisotropy, while CrSeTe has large DMI which favors the formation of chiral Néel domain walls (DWs). They also found that the DW in CrSeTe can be tuned into skyrmion states with an external magnetic field and strain [64].

Finally, the single-ion anisotropy (SIA) parameters of four Cr atoms in the unit cell are calculated individually. Although

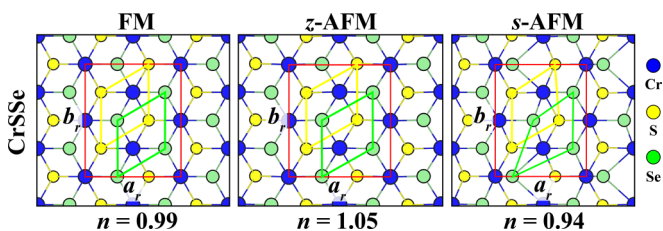


FIG. 5. Top view of the optimized structure of CrSSe for three different magnetic orders: FM, z -AFM, and s -AFM. The yellow (bottom S) and green (top Se) show the ordering. While z -AFM is in nearly perfect 1T form, the s -AFM case presents the most distorted structure (with buckled Cr layer shown in Fig. 1), which exhibits the lowest energy.

we obtained all elements of the 3×3 SIA matrices, necessary in broken structural symmetry in the monolayer, we only list the A_i^{zz} components, as they are mostly the strongest, except for CrTe₂. Our findings indicate that SIA is dominated by isotropic magnetic exchange interactions, which are an order of magnitude lower, thus it is not expected to significantly influence T_c or the temperature-dependent magnetization behavior. Regarding the ground state magnetic moments, MGS, we do not find any notable influence. For example, CrS₂ exhibits $\langle A_i^{zz} \rangle = -0.12$ meV, suggesting a preference for spins to align in the out-of-plane direction, despite exhibiting s-AFM in the x direction. Similar relationships are found in CrSe₂, CrSSe, and CrSTe. Notably, $A_i^{xz} = A_i^{zx}$ for CrTe₂ was found to be -0.25 meV, which induces a canting of the magnetic moment in the xz plane, whereas $\langle A_i^{zz} \rangle = 0.22$ meV favors in-plane alignment of the magnetic moment, even though the MGS is FM (t-xyz), suggesting a small contribution from SIA to the MGS direction. In the case of CrSeTe, the MGS of FM (y) is consistent with $\langle A_i^{zz} \rangle = 0.20$ meV, which prefers an in-plane alignment.

IV. CONCLUSIONS

In summary, we have detailed the structural, electronic, vibrational, and magnetic properties of 2D Janus CrXY ($X, Y = \text{S, Se, Te}$, with $X \neq Y$) monolayer materials and compared them to those of 2D pristine CrX₂ monolayers, using relativistic density-functional calculations, including DFT + U correction, the four-state energy mapping methodology (4SM) to extract all relevant magnetic interactions, and the atomistic spin relaxation to obtain the ground-state spin textures and the critical temperature of the long-range magnetic order. In the Janus CrXY monolayers, where inversion symmetry is broken between different surface chalcogens, the different electronegativities and atomic numbers between chalcogen atoms (X and Y) induce not only changes in the structural parameters compared to those of the pristine 1T-CrX₂, but also the nondegenerated d states of Cr deviate from those in the ideally octahedral crystal field. As a consequence, the type of the dominant $p(\text{chalcogen})-d(\text{Cr})$ interaction will strongly depend on the geometric organization of the chalcogen atoms

around the Cr atom, which in turn influences the electronic structure and magnetic properties of each considered 2D Janus CrXY monolayer.

Concerning the favorable magnetic order, we find that monolayer CrS₂ and CrSe₂ exhibit s-AFM and z-AFM order with critical temperatures T_c of 222 and 52 K, respectively. However, CrTe₂ exhibits tilted FM order, up to T_c of 186 K. As expected there is no DMI found in these pristine dichalcogenide monolayers, due to preserved inversion symmetry. The Janus CrSSe is a FM material, with T_c of 268 K. It should be noted that CrSSe exhibits significantly distorted structure, both in-plane and out-of-plane (i.e., buckled chromium mid-layer), very strongly coupled to the magnetic order. Janus CrSTe and CrSeTe monolayers are also in FM order, with T_c of 319 and 268 K, respectively. Although all structures of the Janus monolayers are significantly distorted, DMI is particularly strong only for monolayer CrSeTe, being 1.21 meV on average, which corresponds to 15% of the average isotropic exchange and suggests possibility of formation of stable non-collinear spin textures with nonzero topological charge (such as magnetic skyrmions). On the other hand, we found that SIA does not significantly influence T_c and MGS of both pristine and Janus monolayers.

The very strong coupling between the spin textures and the lattice structure found in these Cr-based (pristine and Janus) monolayer dichalcogenides, together with their versatile electronic properties (metal or semiconducting), high critical temperature of their magnetic order, as well as the coupling between the magnetic and electronic degrees of freedom (DMI and polarization) with every present symmetry breaking, suggest these materials for further experimental exploration and use in spintronic, sensing, and piezomagneto-electric applications.

ACKNOWLEDGMENTS

This work was supported by the Special Research Funds of the University of Antwerp (BOF-UA), by the Research Foundation-Flanders (FWO), and by Universidad del Norte (UniNorte). The calculations were performed in part using the facilities of the Flemish Supercomputer Center (VSC), funded by the FWO and the Flemish Government, department EWI.

-
- [1] N. D. Mermin and H. Wagner, *Phys. Rev. Lett.* **17**, 1133 (1966).
 - [2] P. C. Hohenberg, *Phys. Rev.* **158**, 383 (1967).
 - [3] W. Cong, Z. Tang, X. Zhao, and J. Chu, *Sci. Rep.* **5**, 9361 (2015).
 - [4] A. González-García, W. López-Pérez, R. González-Hernández, C. Bacaksiz, D. Šabani, M. Milošević, and F. Peeters, *J. Phys.: Condens. Matter* **33**, 145803 (2021).
 - [5] P. V. Ong, N. Kioussis, P. K. Amiri, J. Alzate, K. Wang, G. P. Carman, J. Hu, and R. Wu, *Phys. Rev. B* **89**, 094422 (2014).
 - [6] E. Torun, H. Sahin, C. Bacaksiz, R. T. Senger, and F. M. Peeters, *Phys. Rev. B* **92**, 104407 (2015).
 - [7] B. Huang, G. Clark, E. Navarro-Moratalla, D. R. Klein, R. Cheng, K. L. Seyler, D. Zhong, E. Schmidgall, M. A. McGuire, D. H. Cobden *et al.*, *Nature (London)* **546**, 270 (2017).
 - [8] C. Gong, L. Li, Z. Li, H. Ji, A. Stern, Y. Xia, T. Cao, W. Bao, C. Wang, Y. Wang *et al.*, *Nature (London)* **546**, 265 (2017).
 - [9] L. Chen, C. Mao, J.-H. Chung, M. B. Stone, A. I. Kolesnikov, X. Wang, N. Murai, B. Gao, O. Delaire, and P. Dai, *Nat. Commun.* **13**, 4037 (2022).
 - [10] I. Dzyaloshinsky, *J. Phys. Chem. Solids* **4**, 241 (1958).
 - [11] T. Moriya, *Phys. Rev.* **120**, 91 (1960).
 - [12] M. Hervé, B. Dupé, R. Lopes, M. Böttcher, M. D. Martins, T. Balashov, L. Gerhard, J. Sinova, and W. Wulfhekel, *Nat. Commun.* **9**, 1015 (2018).
 - [13] M. Yagmurcukardes, Y. Qin, S. Ozen, M. Sayyad, F. M. Peeters, S. Tongay, and H. Sahin, *Appl. Phys. Rev.* **7**, 011311 (2020).
 - [14] L. Zhang, Z. Yang, T. Gong, R. Pan, H. Wang, Z. Guo, H. Zhang, and X. Fu, *J. Mater. Chem. A* **8**, 8813 (2020).

- [15] C. Xia, W. Xiong, J. Du, T. Wang, Y. Peng, and J. Li, *Phys. Rev. B* **98**, 165424 (2018).
- [16] R. Li, Y. Cheng, and W. Huang, *Small* **14**, 1802091 (2018).
- [17] V. Van Thanh, N. D. Van, R. Saito, N. T. Hung *et al.*, *Appl. Surf. Sci.* **526**, 146730 (2020).
- [18] A.-Y. Lu, H. Zhu, J. Xiao, C.-P. Chuu, Y. Han, M.-H. Chiu, C.-C. Cheng, C.-W. Yang, K.-H. Wei, Y. Yang *et al.*, *Nat. Nanotechnol.* **12**, 744 (2017).
- [19] J. Zhang, S. Jia, I. Kholmanov, L. Dong, D. Er, W. Chen, H. Guo, Z. Jin, V. B. Shenoy, L. Shi *et al.*, *ACS Nano* **11**, 8192 (2017).
- [20] Z. Guan, N. Luo, S. Ni, and S. Hu, *Mater. Adv.* **1**, 244 (2020).
- [21] J. Liang, W. Wang, H. Du, A. Hallal, K. Garcia, M. Chshiev, A. Fert, and H. Yang, *Phys. Rev. B* **101**, 184401 (2020).
- [22] J. Yuan, Y. Yang, Y. Cai, Y. Wu, Y. Chen, X. Yan, L. Shen *et al.*, *Phys. Rev. B* **101**, 094420 (2020).
- [23] C. Xu, J. Feng, S. Prokhorenko, Y. Nahas, H. Xiang, and L. Bellaiche, *Phys. Rev. B* **101**, 060404(R) (2020).
- [24] Y. Hou, F. Xue, L. Qiu, Z. Wang, and R. Wu, *npj Comput. Mater.* **8**, 120 (2022).
- [25] M. R. Habib, S. Wang, W. Wang, H. Xiao, S. M. Obaidulla, A. Gayen, Y. Khan, H. Chen, and M. Xu, *Nanoscale* **11**, 20123 (2019).
- [26] A. Shivayogimath, J. D. Thomsen, D. Mackenzie, M. Geisler, R.-M. Stan, A. J. Holt, M. Bianchi, A. Crovetto, P. R. Whelan, A. Carvalho *et al.*, *Nat. Commun.* **10**, 2957 (2019).
- [27] J. Sugiyama, H. Nozaki, I. Umegaki, T. Uyama, K. Miwa, J. H. Brewer, S. Kobayashi, C. Michioka, H. Ueda, and K. Yoshimura, *Phys. Rev. B* **94**, 014408 (2016).
- [28] D. C. Freitas, M. Nunez, P. Strobel, A. Sulpice, R. Weht, A. A. Aligia, and M. Nunez-Regueiro, *Phys. Rev. B* **87**, 014420 (2013).
- [29] D. C. Freitas, R. Weht, A. Sulpice, G. Remenyi, P. Strobel, F. Gay, J. Marcus, and M. Núñez-Regueiro, *J. Phys.: Condens. Matter* **27**, 176002 (2015).
- [30] J.-J. Xian, C. Wang, J.-H. Nie, R. Li, M. Han, J. Lin, W.-H. Zhang, Z.-Y. Liu, Z.-M. Zhang, M.-P. Miao *et al.*, *Nat. Commun.* **13**, 257 (2022).
- [31] X. Zhang, Q. Lu, W. Liu, W. Niu, J. Sun, J. Cook, M. Vaninger, P. F. Miceli, D. J. Singh, S.-W. Lian *et al.*, *Nat. Commun.* **12**, 2492 (2021).
- [32] J. He and S. Li, *Comput. Mater. Sci.* **152**, 151 (2018).
- [33] E. C. Ahn, *npj 2D Mater. Appl.* **4**, 17 (2020).
- [34] D. J. P. De Sousa, M. J. Sammon, R. Kim, H. Li, I. A. Young, and T. Low, *Phys. Rev. B* **106**, 184412 (2022).
- [35] P. Hohenberg and W. Kohn, *Phys. Rev.* **136**, B864 (1964).
- [36] W. Kohn and L. J. Sham, *Phys. Rev.* **140**, A1133 (1965).
- [37] J. P. Perdew, K. Burke, and M. Ernzerhof, *Phys. Rev. Lett.* **77**, 3865 (1996).
- [38] P. E. Blöchl, *Phys. Rev. B* **50**, 17953 (1994).
- [39] G. Kresse and D. Joubert, *Phys. Rev. B* **59**, 1758 (1999).
- [40] G. Kresse and J. Furthmüller, *Comput. Mater. Sci.* **6**, 15 (1996).
- [41] G. Kresse and J. Furthmüller, *Phys. Rev. B* **54**, 11169 (1996).
- [42] S. Grimme, *J. Comput. Chem.* **27**, 1787 (2006).
- [43] V. I. Anisimov, J. Zaanen, and O. K. Andersen, *Phys. Rev. B* **44**, 943 (1991).
- [44] M. Cococcioni and S. de Gironcoli, *Phys. Rev. B* **71**, 035105 (2005).
- [45] A. Togo and I. Tanaka, *Scr. Mater.* **108**, 1 (2015).
- [46] G. Kresse, J. Furthmüller, and J. Hafner, *Europhys. Lett.* **32**, 729 (1995).
- [47] K. Parlinski, Z. Q. Li, and Y. Kawazoe, *Phys. Rev. Lett.* **78**, 4063 (1997).
- [48] H. Xiang, C. Lee, H.-J. Koo, X. Gong, and M.-H. Whangbo, *Dalton Trans.* **42**, 823 (2013).
- [49] D. Šabani, C. Bacaksiz, and M. Milošević, *Phys. Rev. B* **102**, 014457 (2020).
- [50] G. P. Müller, M. Hoffmann, C. Dißelkamp, D. Schürhoff, S. Mavros, M. Sallermann, N. S. Kiselev, H. Jónsson, and S. Blügel, *Phys. Rev. B* **99**, 224414 (2019).
- [51] M. J. Varjovi and E. Durgun, *Phys. Rev. Mater.* **5**, 104001 (2021).
- [52] Y. Cheng, Z. Zhu, M. Tahir, and U. Schwingenschlögl, *Europhys. Lett.* **102**, 57001 (2013).
- [53] C. Wang, X. Zhou, Y. Pan, J. Qiao, X. Kong, C.-C. Kaun, and W. Ji, *Phys. Rev. B* **97**, 245409 (2018).
- [54] S. Lebegue, T. Björkman, M. Klintonberg, R. M. Nieminen, and O. Eriksson, *Phys. Rev. X* **3**, 031002 (2013).
- [55] K. Chen, J. Deng, Y. Yan, Q. Shi, T. Chang, X. Ding, J. Sun, S. Yang, and J. Z. Liu, *npj Comput. Mater.* **7**, 79 (2021).
- [56] H. Y. Lv, W. J. Lu, D. F. Shao, Y. Liu, and Y. P. Sun, *Phys. Rev. B* **92**, 214419 (2015).
- [57] X. Yang, X. Zhou, W. Feng, and Y. Yao, *Phys. Rev. B* **103**, 024436 (2021).
- [58] J. Jiao, N. Miao, Z. Li, Y. Gan, J. Zhou, and Z. Sun, *J. Phys. Chem. Lett.* **10**, 3922 (2019).
- [59] B. Zhou, Q. Zhao, Z. Liu, X. Shen, X. Ye, J. Shi, Z. Liao, W. Wang, Z. Hu, H.-J. Lin *et al.*, *NPG Asia Mater.* **12**, 69 (2020).
- [60] H. Yang, S. O. Valenzuela, M. Chshiev, S. Couet, B. Dieny, B. Dlubak, A. Fert, K. Garello, M. Jamet, D.-E. Jeong *et al.*, *Nature (London)* **606**, 663 (2022).
- [61] S. Manzeli, D. Ovchinnikov, D. Pasquier, O. V. Yazyev, and A. Kis, *Nat. Rev. Mater.* **2**, 17033 (2017).
- [62] S. Lee, D. J. P. de Sousa, Y.-K. Kwon, F. de Juan, Z. Chi, F. Casanova, and T. Low, *Phys. Rev. B* **106**, 165420 (2022).
- [63] N. Ontoso, C. K. Safeer, F. Herling, J. Ingla-Aynes, H. Yang, Z. Chi, B. Martin-Garcia, I. Robredo, M. G. Vergniory, F. de Juan, M. Reyes Calvo, L. E. Hueso, and F. Casanova, *Phys. Rev. Appl.* **19**, 014053 (2023).
- [64] Q. Cui, J. Liang, Z. Shao, P. Cui, and H. Yang, *Phys. Rev. B* **102**, 094425 (2020).